

## PROJECT FINAL REPORT

Project Title: Combined Exposures to Ultrafine Particulate Matter and Ozone: Characterization of Particulate Deposition, Pulmonary Oxidant Stress and Myocardial Injury.

Agreement No: 17RD011

Project Period: 01/01/19 through 01/27/22

Submitted to: Hnin-Hnin Aung  
Research Division  
California Air Resources Board  
1001 I Street, 5<sup>th</sup> Floor  
Sacramento, CA 95814

Prepared by: Edward Schelegle, Principal Investigator  
School of Veterinary  
University of California, Davis  
One Shields Avenue  
Davis, CA 95616  
Phone: 530-752-8259  
Email: [esschelegle@ucdavis.edu](mailto:esschelegle@ucdavis.edu)

Disclaimer: The statements and conclusions in this Report are those of the contractor and not necessarily those of the California Air Resources Board. The mention of commercial products, their source, or use in connection to the material reported herein is not to be construed as actual or implied endorsement of such products.

Acknowledgements: We thank Drs. Rachel Reader and Laura Van Winkle, William Walby, and Patricia Edwards for their technical efforts and expertise.

This report was submitted in fulfillment of ARB Contract #17RD011, "Combined Exposures to Ultrafine Particulate Matter and Ozone: Characterization of Particulate Deposition, Pulmonary Oxidant Stress and Myocardial Injury," by UC Davis under the sponsorship of the California Air Resources Board. Work was completed as of July 15, 2021.

This project is funded under the CARB's Dr. William F. Friedman Health Research Program. During Dr. Friedman's tenure on the Board, he played a major role in guiding CARB's health research program. His commitment to the citizens of California was evident through his personal and professional interest in the Board's health research, especially in studies related to children's health. The Board is sincerely grateful for all of Dr. Friedman's personal and professional contributions to the State of California.

## TABLE OF CONTENTS

1. Abstract	1
2. Executive Summary	2
3. Background	3
4. Methods	5
5. Results	9
6. Discussion	14
7. Recommendations	18
8. Glossary of Terms & Abbreviations	19
9. References	20

### List of Figures

Figure 1. Premixed fuel particle generator	6
Figure 2. Representative examples of interstitial expansion and replacement fibrosis	7
Figure 3. UFPM increased microthrombi formation in myocardium and lung	10
Figure 4. UFPM+O <sub>3</sub> increased microthrombi formation in lung	11
Figure 5. UFPM+O <sub>3</sub> increased microthrombi formation in myocardium	12
Figure 6. Myocardial fibrosis in SH rats	13
Figure 7. Integration of results	17

### List of Tables

Table 1. Most abundant PAHs in UFPM and UFPM+O <sub>3</sub> exposure atmospheres	9
Table 2. Histopathological measures of the lung	9
Table 3. Histopathological measures of the myocardium	10

## 1. ABSTRACT

Epidemiologic research has suggested a statistical correlation between exposure to particulate matter 2.5  $\mu\text{m}$  or less in diameter (PM<sub>2.5</sub>) and ozone (O<sub>3</sub>), and adverse health effects. Findings obtained from our recent investigation, "Co-Exposure to PM (UFPM) and O<sub>3</sub>: Pulmonary C Fiber Platelet Activation in Decreased HRV," demonstrated that simultaneous exposure to a combination of ultrafine particulate matter (UFPM) 0.1  $\mu\text{m}$  or less in diameter and O<sub>3</sub> increases the biological potency of exposure, resulting in exaggerated pulmonary and cardiac patho-physiological responses compared to single pollutant exposure in mature adult rats with (spontaneous hypertensive, SH) and without (Wistar-Kyoto, WKY) cardiovascular disease (CVD). Our observations are consistent with an integrated response, which is initiated in the lung, and results in downstream hematological and autonomic nervous system responses that manifest in the heart as increased arrhythmias, decreased heart rate variability, and myocardial injury in mature adults with CVD. Importantly, this is the first study to provide direct evidence of air pollution exposure-induced myocardial injury in an animal model. The current study examined lung and heart tissue collected in our initial study to determine whether UFPM+O<sub>3</sub>; 1) induced myocardial ischemia and nonapoptotic cell death; 2) increased microthrombi in lung and heart; and 3) altered UFPM deposition and its relation to cellular antioxidant expression within the airways. While the time of tissue collection (8 hours post-exposure) and the method of fixation (airway) were appropriate for evaluating airway injury and inflammation in our initial study, they severely limited the ability to examine myocardial ischemia, nonapoptotic cell death, UFPM deposition as well as exposure-induced cellular antioxidant expression. Cardiac fibrosis was significantly greater in SH compared to WKY rats, but there was no exposure-related effect, indicating that the increased fibrosis is a marker of previous injury in SH rats. Microthrombi in the lungs and heart, assessed as fibrin-stabilized aggregates, were present in SH and WKY rats exposed to UFPM and UFPM+O<sub>3</sub>. UFPM+O<sub>3</sub> resulted in more microthrombi with more severe vascular occlusion compared to UFPM; furthermore, SH rats had more microthrombi with more severe vascular occlusion with UFPM and UFPM+O<sub>3</sub> exposure compared to WKY rats. Our data indicates that simultaneous exposure to UFPM and O<sub>3</sub> is increasingly toxic, eliciting stronger responses than that expected from exposure to O<sub>3</sub> or UFPM alone; and further, CVD increases susceptibility to pollutant-induced thrombosis, which may contribute to UFPM+O<sub>3</sub> induced myocardial injury we observed previously. This work improves scientific understanding of the adverse effects of simultaneous combined-pollutant exposure and provides novel insight into the association between ambient air pollution and increased cardiac mortality in mature adult individuals with CVD. This will aid CARB in developing and evaluating air pollution standards.

## 2. EXECUTIVE SUMMARY

**Background:** Many observational and epidemiological studies have consistently demonstrated that exposure to particulate matter 2.5  $\mu\text{m}$  or less in diameter (PM<sub>2.5</sub>) is associated with increased cardiovascular (CV) morbidity and mortality, especially in individuals with underlying cardiovascular disease (CVD). Short term (acute) PM<sub>2.5</sub> exposures have been associated with excess CV-related hospitalizations and deaths from myocardial ischemia, heart failure, and arrhythmias (1, 2). It has been proposed that ultrafine particulate matter (UFPM) 0.1  $\mu\text{m}$  or less in diameter have greater adverse CV effects due to their large reactive surface area and their ability to penetrate the alveoli and translocate into the vasculature. To better understand of the mechanisms responsible for increased CV risk in older populations exposed to UFPM and the oxidant air pollutant ozone (O<sub>3</sub>) in combination, we examined the cardio-pulmonary pathophysiological responses of mature adult rats with (Spontaneous Hypertensive, SH) and without (normotensive Wistar-Kyoto, WKY) preexisting CVD (3). Data from this initial study is consistent with the simultaneous exposure to UFPM and O<sub>3</sub> being increasingly toxic, eliciting stronger responses than that expected from exposure to O<sub>3</sub> or UFPM alone; and with CVD increasing susceptibility to pollutant-induced lung and heart injury. The current study was undertaken to extend our observations and further aid the development of air pollution regulatory strategies.

**Objectives:** The objectives of this study were designed to test the hypothesis, that *O<sub>3</sub> enhances the biologic potency of UFPM by promoting ROS production at the particle surface, altering UFPM chemical composition; exposure to which increases cellular antioxidant expression, and promotes platelet-leukocyte and platelet-neutrophil interactions. Furthermore, mature adult SH rats are more sensitive to oxidants, and thus, more susceptible to microthrombi formation and myocardial damage following exposure.*

**Methods:** Pulmonary and cardiac tissue collected in our previous study from mature adult male WKY and SH rats were evaluated in this study. Rats were exposed to one of the following experimental atmospheres: filtered air (FA), 250  $\mu\text{g}/\text{m}^3$  ultrafine particulate matter (UFPM), 1.0 ppm O<sub>3</sub>, or 250  $\mu\text{g}/\text{m}^3$  UFPM and 1.0 ppm O<sub>3</sub> (UFPM+O<sub>3</sub>) simultaneously. This experimental design resulted in 8 groups of rats (2 rat strains x 4 experimental atmospheres = 8 groups). Each group consisted of 5-7 rats; a total of 50 rats were studied. We examined: 1) the cellular expression of JunB, an early marker of myocardial ischemia, and Nur77, a marker of nonapoptotic cell death, in order to determine whether UFPM+O<sub>3</sub> induced cardiac lesions resulted from an ischemic event; 2) cardiac fibrosis as a marker of chronic injury using Masson's trichrome histochemical staining; 3) microthrombi present in the heart and lung using phosphotungstic acid-hematoxylin histochemical staining; and 4) the relationship between UFPM deposition and cellular oxidative stress within the airways using hyperspectral imaging of lung tissue dual-stained for Nrf2-dependent phase II antioxidants hemeoxygenase-1 and superoxide dismutase.

**Results:** Cardiac fibrosis was significantly greater in SH compared to WKY rats; however, there was no exposure related effect, indicating that the increased cardiac fibrosis is a marker of previous injury in SH rats. Microthrombi in the heart and lungs assessed as fibrin-stabilized aggregates were present in SH and WKY rats exposed to UFPM and UFPM+O<sub>3</sub>. UFPM+O<sub>3</sub> resulted in more microthrombi with more severe vascular occlusion compared to UFPM. Furthermore, SH rats had more microthrombi with more severe vascular occlusion with UFPM and UFPM+O<sub>3</sub> exposure compared to WKY rats. These observations support our previous observation that mature adult animals with pre-existing CVD are more susceptible to UFPM induced prothrombotic effects as assessed by platelet activation and at greater risk for vascular occlusion in the heart and lungs resulting from exposure to either UFPM or UFPM+O<sub>3</sub>.

**Conclusions:** These data provide additional critical information regarding the risks of simultaneous pollutant exposure (UFPM+O<sub>3</sub>) in mature adults with underlying CVD as well as mechanisms of disease in these populations. Our data is consistent with the combined pollutant atmosphere being more toxic than would be expected from the responses elicited by O<sub>3</sub> and UFPM alone and with chronic CVD increasing the susceptibility to pollutant-induced lung and heart injury. Using a rat model of CVD in mature adults this work improves the scientific understanding of the adverse effects of simultaneous combined-pollutant exposure and provides possibly important insight into the association between ambient air pollution and increased cardiac morbidity and mortality. This will aid CARB in developing and evaluating air pollution standards in the context of the exacerbated adverse cardiovascular events that are induced by the combined exposure to O<sub>3</sub> and UFPM in

individuals with preexisting cardiovascular disease and highlights the need to develop an ambient air pollution metric that better predicts the adverse health effects induced by combined pollutant exposure. This might require targeted controlled human and animal exposure studies, as well as new epidemiology studies that focus on pollutant interactions and their effects on cardiovascular and other outcomes.

### **3. BACKGROUND**

Older individuals with pre-existing cardiovascular disease (CVD) are more susceptible to air pollution, and at greater risk for cardiovascular (CV) events, including stroke, myocardial ischemia, infarction, and sudden death following short-term exposure (2, 4). Importantly, aging is widely accepted as a premier risk factor for CVD, thus the prevalence CVD will likely increase as the U.S. population ages. In fact, it is estimated that by the year of 2030, nearly half of the U.S. adult population will have some form of CVD (5). Thus, air pollution is a growing threat to public health that will increasingly burden health care and economic resources. Therefore, better scientific understanding of the biologic mechanisms underlying the link between air pollution and CV events air pollution is required to limit future impacts.

Air pollution is a complex heterogeneous mixture of particles and gases, arising from a wide range of sources. Of the major air pollutants, particulate matter (PM) and ozone (O<sub>3</sub>) are the most ubiquitous and strongly correlated with cardiopulmonary morbidities and mortalities (6-8). Although both PM and O<sub>3</sub> affect the cardiopulmonary system (8), fine (PM<sub>2.5</sub>, aerodynamic diameter < 2.5 μm) and ultrafine particulates (PM<sub>0.1</sub>, aerodynamic diameter < 0.1 μm) are the most consistently associated with adverse health effects (9, 10). Atmospheric interactions between PM and O<sub>3</sub> may have additive exposure-related health effects (11, 12). As a potent oxidant, O<sub>3</sub> readily reacts with chemical constituents adsorbed onto the PM surface, specifically, polycyclic aromatic hydrocarbons (PAHs), yielding a complex mixture of reactive oxygen species (ROS), including hydroxyl radicals, aldehydes, carboxylic acids, and hydrogen peroxides, at the particle surface (13). Previous studies have demonstrated that ozonation of PM increases the biologic potency of exposure (14, 15). Because vehicular exhaust is the dominant contributor of atmospheric PM<sub>0.1</sub> and PM<sub>2.5</sub>, as well as a primary source of O<sub>3</sub>, reactions between PM and O<sub>3</sub> are particularly relevant in areas with high traffic.

ROS generated from PM is implicated in the induction of oxidative stress; a key pathway by which PM exerts cardiovascular effects (16, 17). Oxidative stress occurs upon loss of homeostasis, where ROS generation overwhelms antioxidant defenses. At the cellular level, this results in cytotoxicity (18) and the activation of specific transcriptional pathways, including Nrf2, which is responsible for upregulating phase II antioxidant gene expression (19). These inducible antioxidant enzymes are critical for reducing intracellular ROS, and restoring cellular homeostasis. Critically, oxidative stress elicits and is induced by inflammatory processes; the two activities are biologically linked. Inhalation of PM, therefore, initiates both oxidative stress and inflammatory responses. The inflammatory response to PM is characterized by the production of pro-inflammatory and pro-thrombotic cytokines, which ultimately, leads to the development of a pro-thrombotic state. Both human and animal studies have shown that inhalation of PM increases platelet activation, platelet-leukocyte and platelet-monocyte interactions, as well as decreased fibrinolysis – all of which are predisposing factors for thrombus formation potentially resulting in stroke, myocardial ischemia, or myocardial infarction (20-22).

#### **Previous Findings (CARB Contract #13-311)**

We completed a study (3) designed to examine the upstream events associated with air pollutant induced CV adverse events. Mature adult rats with (Spontaneously Hypertensive; SH) and without (normotensive Wistar-Kyoto; WKY) preexisting CVD were used in this study to mirror the epidemiologic data. Prior to the study, animals were instrumented with telemeters to enable the study of the electrocardiogram (ECG) while awake and ambulatory. Once animals recovered from surgery (two-week minimum) animals were exposed to either filtered air (FA), ~250 ug/m<sup>3</sup> ultrafine particulate matter (UFPM), 1.0 ppm O<sub>3</sub>, or ~250 ug/m<sup>3</sup> UFPM and 1.0 ppm O<sub>3</sub> simultaneously (UFPM+O<sub>3</sub>) for 6 hours followed by an 8-hour recovery period prior to euthanasia. ECG data were obtained through the exposure and recovery periods and evaluated for arrhythmias and alterations in heart rate variability (HRV). Both peripheral blood and tissues were obtained at the time of euthanasia for further analysis. Flow cytometry was used to determine platelet activation as well as platelet-white blood cell interactions; a reflection of systemic inflammation. Lung and heart tissue was histologically examined to determine if there were adverse effects associated with exposure. Results from this study were as follows:

- O<sub>3</sub> reacts with polycyclic-aromatic hydrocarbons (PAHs) contained in combustion-derived UFPM to produce a potentially more toxic profile of oxidant-derived reaction products.
- The co-pollutant UFPM+O<sub>3</sub> atmosphere induced significantly greater changes in airway injury, inflammation, alterations of HRV, and arrhythmias than UFPM or O<sub>3</sub> atmosphere alone in mature adult animals with or without CVD.
- Mature adult animals with CVD are more susceptible to oxidant injury induced by O<sub>3</sub> compared to age matched animals without CVD as indicated by greater inflammation, airway injury and alterations in HRV.
- The co-pollutant UFPM+O<sub>3</sub> atmosphere induced significantly greater changes in platelet activation, platelet microvesicles as well as platelet-white blood cell aggregation. These parameters lay the foundation for a pro-coagulant and pro-inflammatory systemic vascular environment.
- Mature adult animals with CVD exposed to the co-pollutant UFPM+O<sub>3</sub> atmosphere develop myocardial injury despite having similar changes in HRV, and arrhythmias as age-matched animals without CVD.
- Evidence is consistent with an integrated response to the co-pollutant UFPM+O<sub>3</sub> atmosphere that is initiated in the lung, results in downstream hematological and autonomic nervous system responses that manifests as increased platelet activation and arrhythmias, decreased HRV and myocardial injury in mature adults with CVD.

Overall, our data from our previous study (3) strongly suggested that underlying CVD in mature adult populations may be an important factor in the response to exposure to O<sub>3</sub> as well as to UFPM and O<sub>3</sub>. Notably, this was the first study to provide evidence of air pollution exposure-induced myocardial necrosis in an animal model.

#### **Objectives of Current Study (CARB Contract #17RD011)**

The objective of the present study was to better understand our previous findings and address the overall hypothesis that: *O<sub>3</sub> enhances the biologic potency of UFPM by promoting ROS production at the particle surface, altering UFPM chemical composition; exposure to which increases cellular antioxidant expression, and promotes platelet-leukocyte and platelet-neutrophil interactions. Furthermore, mature adult SH rats are more sensitive to oxidants, and thus, more susceptible to microthrombi formation and myocardial damage following exposure.*

#### **Objective 1. Define the effect of O<sub>3</sub> on the local relationship between particle deposition and cellular oxidative stress within the airways.**

*Rationale:* We previously demonstrated that UFPM+O<sub>3</sub> induced greater airway injury and inflammation in WKY and SH rats compared to UFPM and O<sub>3</sub> alone (3). To determine the impact of particulate deposition on injury and inflammation in the lung, particles and cellular antioxidant expression were investigated by examining their spatial proximity and organization.

*Approach:* Enhanced darkfield microscopy complemented with a hyperspectral imaging system was used to examine lung tissue double-stained for Nrf2-dependent phase II antioxidants hemoxygenase-1 (HMOX1) and superoxide dismutase-1 (SOD1), with the objective of visualizing the particles and cellular markers of oxidant stress and metabolism simultaneously, and evaluate their spatial proximity and organization.

#### **Objective 2. Characterize UFPM+O<sub>3</sub> impact on microthrombi formation.**

*Rationale:* We previously demonstrated that UFPM+O<sub>3</sub> induced changes in platelet activation, and platelet-white blood cell aggregation (3). However, it is unclear whether these changes lead to microthrombi stabilization and deposition in the lung and heart.

*Approach:* We examined lung and myocardial tissue obtained from our previous study for microthrombi using a histochemical stain, phosphotungstic acid-hematoxylin (PTAH) to stain fibrin-stabilized aggregates.

#### **Objective 3. Define UFPM+O<sub>3</sub> impact on myocardial injury.**

*Rationale:* We previously demonstrated that mature adult SH rats exposed to either UFPM alone or in combination with O<sub>3</sub> displayed acute myocardial changes, including acute cellular necrosis, and hypercontractility (3). While these changes are often associated with ischemic injury, the nature of the injury was not assessed.

*Approach:* To determine whether the previously observed cardiac lesions resulted from an ischemic event, we examined myocardial tissue obtained from our previous study for cellular expression of JunB, an early marker of

myocardial ischemia, and Nur77, a marker of nonapoptotic cell death. We also characterized cardiac fibrosis (CF), a marker of chronic injury associated with CVD progression, using Masson's trichrome histochemical staining.

#### 4. METHODS

**Animals and housing.** This study adheres to the Animal Research: Reporting of In Vivo Experiments guidelines for animal research (23). The Institutional Animal Care and Use Committee at the University of California, Davis approved this study following guidelines mandated by the U.S. Federal Government (24). Age-matched, mature adult male WKY and SH rats were delivered from the vendor (Envigo, Indianapolis, IN) and housed in filtered air in facilities approved by the American Association for Accreditation of Laboratory Animal Care. Rats were housed in a temperature- ( $22.0 \pm 1.0^\circ$ ) and humidity-controlled ( $55.0 \pm 5\%$ ) room with a 12 h light/dark cycle and air turnover 10 times per h.

**Telemetry implantation.** Rats were acclimated for at least five days in vivarium following delivery prior to undergoing surgical procedures. Rats were fasted for a minimum of 12 h prior to surgery. Prior to surgical procedures, rats were placed in a 10 L glass chamber and anesthesia was induced using 5% isoflurane and maintained through surgical procedures with 3-5% isoflurane (Abbott Laboratories, USA). A ~0.25 ml blood sample was obtained from a tail vein and analyzed for platelet and white blood cell counts. Rats were then treated with meloxicam (2 mg/kg, subcutaneous), a nonsteroidal anti-inflammatory for pain prevention, enrofloxacin (5 mg/kg, intramuscular), a fluoroquinolone antibiotic to prevent bacterial infection, and ophthalmic lubricant was applied to each eye. Abdominal, intercostal and femoral regions were shaved and skin surfaces were deeply scrubbed with a betadine solution to sterilize the area. Following injections, and at least 10 min prior to surgery, incision sites were treated with bupivacaine (5 mg/ml, total volume  $\leq 0.25$  ml), a local anesthetic for pain prevention. A 4-5 cm midline abdominal incision was made in the skin starting at the xiphoid and subcutaneous channels for the telemeter leads were formed using blunt dissection. A 2.0-2.5 cm incision was then made in the linea alba again starting at the xiphoid. A two-lead biopotential telemeter (TR50B Millar, Inc) was then placed in the abdominal cavity and secured to the lower abdominal wall using soluble suture. Incision in the linea alba was closed using monofilament suture and 10-15 cm of telemeter lead wire exited the closed incision near the xiphoid. Telemeter leads were secured using silk suture to the fascia covering the cranial portion of the sternum and the right eighth to tenth rib dorsal to the insertion of rectus abdominis. ECG signal quality was examined once telemeter leads were secured. These sites were chosen to minimize artifact associated with breathing and movement and produced a signal comparable to an aV2R ECG lead. Each procedure lasted ~45 min. Rats were placed in a heated cage at  $\sim 37^\circ\text{C}$  upon procedure completion, and then, individually housed in standard rat cages after their health condition was assured. Rats were monitored intermittently and administered analgesic therapies (see above) as well as buprenorphine (Buprenorphine [0.03 mg/kg], Par Pharmaceutical), an opioid narcotic for pain prevention, twice daily for two days following procedure. On the third day, if health condition was assured, rats were re-housed in vivarium, and monitored twice daily for the remainder of their recovery. Rats recovered for a minimum of two wks prior to undergoing experimental exposure.

**Experimental exposure protocol.** Age-matched mature adult WKY and SH rats were randomly assigned to one of the four experimental exposure groups one wk prior to study. Baseline characteristics of each group were reported previously (25). On the day of study, rats were transferred into a standard rodent cage with an open wire mesh top with a perforated Teflon plate inserted ~1 inch above bottom of the standard cage. Rats were placed in exposure chamber at least 1 h prior to exposure protocol. Rats underwent a whole-body exposure to one of the following experimental atmospheres: filtered air,  $\sim 250 \mu\text{g}/\text{m}^3$  UFPM, 1.0 ppm  $\text{O}_3$ , or  $\sim 250 \mu\text{g}/\text{m}^3$  UFPM and 1.0 ppm  $\text{O}_3$  (UFPM+ $\text{O}_3$ ) simultaneously. The experimental protocol was: (1) 1-hour FA control period, (2) 6-hour exposure period, and (3) 8-hour FA recovery period. Immediately following recovery period ( $\sim 8:00$  am, PST), rats were anesthetized as described above (see **Telemetry implantation**), telemetry devices were removed, and animals were necropsied. Rats had *ad libitum* access to food (Laboratory Rodent Diet 5001, LabDiet, St. Louis, MO) and water throughout exposure protocol. Protocols began at  $\sim 5:00$  pm (PST) and concluded the following morning at  $\sim 8:00$  am (PST); standard vivaria ambient room temperature ( $\sim 22^\circ\text{C}$ ) and 12-hour light/dark cycle were maintained.

**Particle generation and monitoring.** Particles were generated using a co-annular premixed flame burner (illustrated in Fig. 1) (30). The burner consists of a 7.1- mm tube (inner diameter) surrounded by an 88.9-mm concentric outer tube (inner diameter) and is enclosed in a Pyrex tube to isolate the burner from ambient air. A mixture of ethylene, oxygen, and argon was metered through the inner tube using mass flow controllers (model 647C flow control unit and model 1179A and M100B flow control valves, MKS Instruments, Andover, MA). A small flow rate of oxygen flowed through the outer annulus to stabilize the flame. The flame was shielded from room air by a curtain flow of nitrogen metered using a Fisher and Porter variable area flow meter (Andrews Glass, Vineland, NJ) and delivered around the circumference of the burner chamber. Filtered, dried air was added to the flow downstream of the flame, and all burner effluent passed through a heated 3-way catalyst to remove NO<sub>x</sub> and CO. Flame-generated particles were diluted with clean, high-efficiency particulate absorbing- and chemical, biological, and radiological-filtered air, before entering the inhalation exposure chamber. Chamber CO levels were monitored using a Teledyne-API Model 300E CO analyzer (San Diego, CA) and was calibrated with an NIST traceable span gas of 202.4 ppm CO diluted in ultrapure air to 10 ppm CO for calibration (Scott-Marrin Inc., Riverside, CA). Chamber NO<sub>x</sub> levels were monitored (Dasibi 2108 Chemiluminescence NO<sub>x</sub> Analyzer, Glendale, CA). PFP was collected directly from the exposure chamber for analysis through ports in the chamber wall. Particle number concentration was determined using a condensation particle counter (CPC, TSI model 3775, Shoreview, MN). Particle size distribution was determined using a scanning mobility particle sizer (SMPS) (model 3080 electrostatic classifier with model 3081 differential mobility analyzer) and a model 3020 CPC (TSI). PFP mass concentration was determined by collecting particles from the chamber on glass fiber filters (Pallflex Emfab 47-mm filters, Ann Arbor, MI) placed in a filter housing (BGI, Waltham, MA). The sampling flow rate was set at 20 L/min air flow rate driven by a vacuum source downstream of the flow. Collection was performed for the duration of the exposure. Total particulate mass was determined gravimetrically (Sartorius AG MC5 microbalance, Goettingen, Germany). Particle samples were collected on 47-mm glass fiber filters (Pallflex Tissuequartz, Ann Arbor, MI) for elemental carbon to organic carbon ratio (EC/OC) analysis as described above. The EC/OC ratio was determined using a method previously described (26).

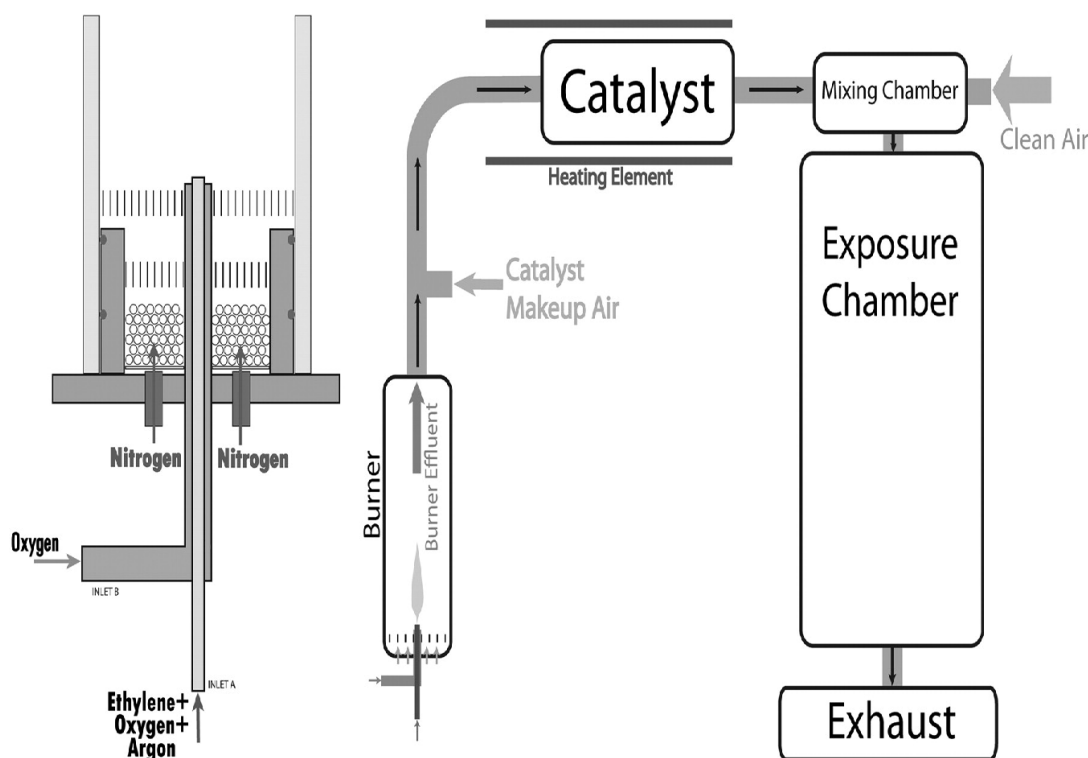


**Figure 1.** Particulate matter generator.

by acetone using an accelerated solvent extractor (Dionex, ASE-300, Salt Lake City, UT). After extraction, samples were pre-concentrated with a rotary evaporator, filtered, exchanged with toluene, and concentrated to 0.1 ml volumes under ultra-high purity nitrogen stream. The extracts were then analyzed using a Varian CP-

**Particle composition.**

Particle and vapor phase PAH speciation was performed by the Organic Analytical Laboratory at the Desert Research Institute (DRI, Reno, NV). Briefly, UFPM+O<sub>3</sub> samples were collected on Pallflex Tissuequartz 47mm filters, and vapor phase organic compounds were collected on XAD resin supplied by DRI. Samples were analyzed for 115 PAH and nitro, oxo-PAH compounds. Filters and XAD-4 resin were spiked with several deuterated PAH internal standards and extracted with dichloromethane followed

3800 GC equipped with a CP-8400 auto-sampler and interfaced to a Varian 4000 Ion Trap Mass Spectrometer (Varian, Inc. Walnut Creek, CA). The limit of quantification (LOQ) values range between 0.025 and 0.082 ng/mL.

**Histopathology.** At necropsy, tracheas were cannulated, the thorax was opened, heart and lungs were removed *en bloc* and fixed with neutral buffered 10% formalin by intratracheal instillation at a controlled pressure of 20 cm hydrostatic pressure for 1 hour at room temperature (RT), trachea was then tied off and allowed to fix overnight at 4°C. Hearts were separated from the lungs, and the lungs were stored in 70% ethanol at 4°C. Hearts were bisected from the base to apex at the coronal plane thereby dividing it into two portions (dorsal and ventral) that each included both right and left ventricles and atria then stored in 70% ethanol until embedded in paraffin, and sectioned. The left and right medial lung lobes were isolated, dissected to expose the airways, embedded in paraffin, and sections. Sections of the heart were stained with either Masson's trichrome, phosphotungstic acid-hematoxylin (PTAH), or using immunohistochemical procedures (described below). Sections of the left lung lobe were stained with PTAH while sections of the right medial lobe were stained using immunohistochemical procedures. A total of eight cardiac sections (two slides/staining procedure), and six lung sections were prepared and assessed for each animal studied. Sections were coded using random sequencing and evaluated without knowledge of animal strain or group assignment.

**Masson's trichrome.** Fibrotic lesions in the heart were assigned a severity score from 0 to 5 based on extent of interstitial expansion and replacement fibrosis observed in each section by a board certified veterinary pathologist, Dr. Rachel Reader, DVM, Diplomate ACVP, PhD (27). Numeric scores correlated with no interstitial expansion (0), minimal multifocal interstitial expansion (1), one or more larger network of mild interstitial expansion (2), one to three networks of mild interstitial expansion with minimal replacement fibrosis (3), three or more networks of interstitial expansion with moderate replacement fibrosis (4), or multiple networks of extensive interstitial expansion with severe replacement fibrosis (5). Figure 2A depicts minimal multifocal interstitial expansion (score = 1). Figure 2B depicts a lesion characterized by extensive interstitial expansion with severe replacement fibrosis (box); samples containing three or more equally severe lesions received a score of 5.

**PTAH.** Vascular occlusion by microthrombi in the lung and heart was examined using phosphotungstic acid-hematoxylin (PTAH) to stain for stabilized fibrin that along with platelets and leukocytes compose microthrombi. Sections of the left lung lobe, as well as the left ventricle and interventricular septum of the heart, were assessed for presence of fibrin-stabilized aggregates by Dr. Emily M. Wong, PhD. Aggregates were classified as one of the following: a small aggregate within small arteriole, medium, or large artery (category I), an aggregate fully occluding a small arteriole (category II), or a large, multifocal aggregate within medium or large artery (category III). The total number of aggregates, within a single sample, were counted for each category. Categories were assigned a score of 0 to 5 correlating with the total number of aggregates observed as follows: none (0), one to three (1), four to six (2), seven to nine (3), ten to twelve (4), or thirteen or more (5) aggregates. Three sections of heart and/or lung tissue were examined, however, only one was selected for statistical analysis.

**Immunohistochemistry.** Sections of heart were immunostained for Nur77, a marker of nonapoptotic cell death, or JunB, an early marker of myocardial ischemia, while sections of the right medial lung lobe were stained for either HMOX1 or SOD1 using histochemical procedures as previously described (28). Briefly, an antigen

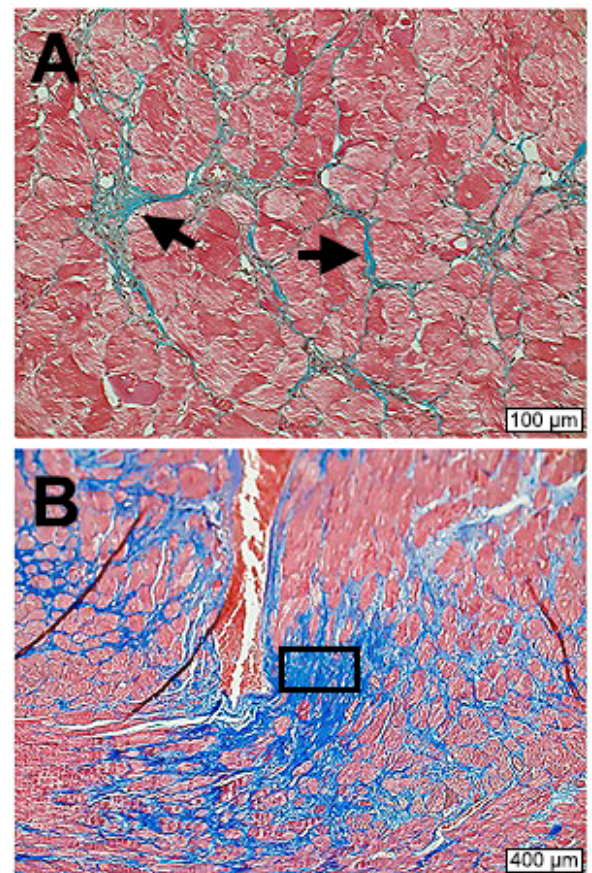


**Figure 2.** Representative images of myocardial fibrotic lesions in SH rat. (A) Minimal multifocal interstitial expansion present as light blue striations (arrows) between myocytes (red). (B) Severe replacement fibrosis presents as blue (box) indicating absence of myocytes (red).

unmasking solution, citric acid based (H-3300; Vector Laboratories, Burlingame, CA) and decloaking chamber (BioCare Medical, Concord, CA) were used for better epitope retrieval. Signals will be amplified using the Vectastain IgG Avidin-Biotin-HRP Kit (Vector Labs, Burlingame, CA) and visualized using nickel chloride-enhanced 3,3'-diaminobenzidine tetrachloride (Sigma Chemical, St. Louis, MO) as the chromogen. Controls were obtained by substituting the primary antibodies with phosphate-buffered saline to ensure specific positive staining. Sections from all groups were run together for each antibody to minimize run-to-run variability. In the heart, the number of Nur77- or JunB-positive cell clusters within the left ventricle and interventricular septum were counted and recorded. Lung sections contained approximately three to five airways, and the number of HMOX-1 and/or SOD1-positive cell clusters within the airway epithelium were counted and recorded per airway cross section.

**Hyperspectral mapping.** Immuno-stained and unstained sections of the medial lung lobe were examined using enhanced darkfield microscopy complemented with a hyperspectral imaging system to visualize particles within the lung. Briefly, a CytoViva Hyperspectral Imaging system mounted on an Olympus BX-43 microscope with an Enhanced Dark-Field Microscopy condenser was used to locate and identify UFPM within the terminal bronchioles of the lung. Positive control samples were analyzed first to generate reference spectra enabling detection of UFPM within samples. Negative controls were analyzed to improve detection specificity (reduce false positives). Samples were imaged and analyzed using methods and software for hyperspectral microscopy or matched against the reference spectra to provide maps of the location of UFPM within each sample.

**Data and statistical analysis.** The total number (*N*) of rats was 5-7 per strain-related exposure group. All data are expressed as mean  $\pm$  SEM. Data were analyzed using SPSS Statistics v. 27 (IBM, Armonk, NY). *p*-Values of 0.05 were considered statistically significant. All data were assessed for significance using a nonparametric Kruskal-Wallis test with Dunn-Bonferroni post hoc comparisons to identify significant differences between exposure groups distinguished by strain. In addition, the nonparametric Mann-Whitney test was used to detect significant differences between strains overall and within each experimental exposure group.

## 5. RESULTS

### OBJECTIVE 1. Define the effect of O<sub>3</sub> on the local relationship between particle deposition and cellular oxidative stress within the airways.

#### O<sub>3</sub> Alters UFPM Chemical Composition

UFPM and UFPM+O<sub>3</sub> atmospheres contained both vapor and particulate phase PAHs (Table 1). In general, methyl biphenyls dominated both the vapor and particulate phases of both atmospheres. Notably, naphthalene and its derivatives were identified in both vapor and particulate phases of UFPM, but not UFPM+O<sub>3</sub>. Furthermore, pyrene, a U.S. EPA “Priority Pollutant,” was abundant in the vapor phase of UFPM+O<sub>3</sub>, but absent in UFPM. These results demonstrate that O<sub>3</sub> dramatically altered the chemical composition of UFPM, indicating the UFPM and UFPM+O<sub>3</sub> atmospheres are not comparable. Therefore, we assessed the significance of UFPM-related effects separately from those of O<sub>3</sub> and UFPM+O<sub>3</sub> using nonparametric comparisons (described above).

#### Particle Deposition

Previously, we predicted that UFPM particles deposit within the terminal bronchiolar region of the lung using the Multiple Path Particle Deposition (MPPD v3.04; Applied Research Associates, Albuquerque, NM) (25). However, we found no UFPM-particles deposited within the terminal bronchiolar or alveolar duct regions using hyperspectral analysis. Specifically, few samples contained particles matching control sample reference spectra. The few particles observed, however, were deposited in the parenchyma, not the terminal bronchioles or alveolar ducts.

#### Cellular Oxidative Stress

We found no significant exposure- or strain-related differences in cellular expression of either HMOX1, a marker of oxidative stress, or SOD1, a marker of superoxide metabolism, within the airway epithelium (Table 2).

**TABLE 1**  
Most Abundant PAHs in UFPM and UFPM+O<sub>3</sub>  
Exposure Atmospheres

UFPM	
Compound	Abundance (ng/m <sup>3</sup> )
2-methylbiphenyl	114.68
3-methylbiphenyl	64.30
2-methylnaphthalene	35.86
1,3+1,6+1,7dimethylnaphthalene	23.78
Naphthalene	18.73
1-methylnaphthalene	17.51
Naphthalene ( <i>p</i> )	15.37
2,6+2,7dimethylnaphthlene	14.22
2-methylnaphthalene ( <i>p</i> )	13.84
1+2ethylnaphthalene	12.61
Fluorene	11.54
UFPM+O <sub>3</sub>	
3-methylbiphenyl	73.12
2-methylbiphenyl	35.87
Pyrene	30.35
4-methylbiphenyl	20.70
Anthrone ( <i>p</i> )	19.32
1+2ethylnaphthalene	19.31
Coronene ( <i>p</i> )	17.94
Benzo[b]chrysene ( <i>p</i> )	16.56
7,12 dimethylbenz[a]anthracene ( <i>p</i> )	13.80

Note: Vapor and particulate (*p*) phase compounds are listed. Compounds identified in samples below detection limits are not listed.

**TABLE 2**  
Histopathological Measures of the Lung

Parameter	WKY				SH			
	FA	UFPM	O <sub>3</sub>	UFPM+O <sub>3</sub>	FA	UFPM	O <sub>3</sub>	UFPM+O <sub>3</sub>
HMOX1	1.3 ± 0.3	1.2 ± 0.3	1.4 ± 0.3	1.4 ± 0.3	1.4 ± 0.4	1.3 ± 0.5	1.3 ± 0.5	1.3 ± 0.4
SOD1	1.2 ± 0.4	1.3 ± 0.5	1.5 ± 0.4	1.6 ± 0.3	1.2 ± 0.3	1.2 ± 0.6	1.1 ± 0.4	1.2 ± 0.4
Fibrin-Stabilized Microthrombi								
Category I	0.0	1.0 ± 0.2*	0.4 ± 0.2	1.2 ± 0.2*†	0.1 ± 0.1	1.9 ± 0.3*§	0.9 ± 0.3	2.5 ± 0.3*†§
II	0.0	0.7 ± 0.2*	0.0	0.6 ± 0.2*†	0.1 ± 0.1	1.1 ± 0.3*	0.5 ± 0.2	1.6 ± 0.2*†§
III	0.0	0.0	0.0	0.1 ± 0.1	0.0	0.4 ± 0.2	0.0	0.6 ± 0.2*†§

Note: Sections of the lung were evaluated histologically for microthrombi; or immunohistochemically for HMOX1, a marker of oxidative stress, or SOD1, a marker of superoxide metabolism, within the airway epithelium. Lung sections contained approximately three to five airways, and the number of HMOX-1 and/or SOD1-positive cell clusters within the airway epithelium were counted and recorded per airway section. Microthrombi scores (scale: 0 to 5) were given based on number of aggregates observed per category per lung section for each animal. Values are shown as the means ± SEM within strain-related exposure groups. *p*-Values ≤ 0.05 were considered significant. \*Significant difference compared to FA within strain-related exposure groups. †Significant difference compared to O<sub>3</sub> within strain-related exposure groups. §Significant difference between strains within

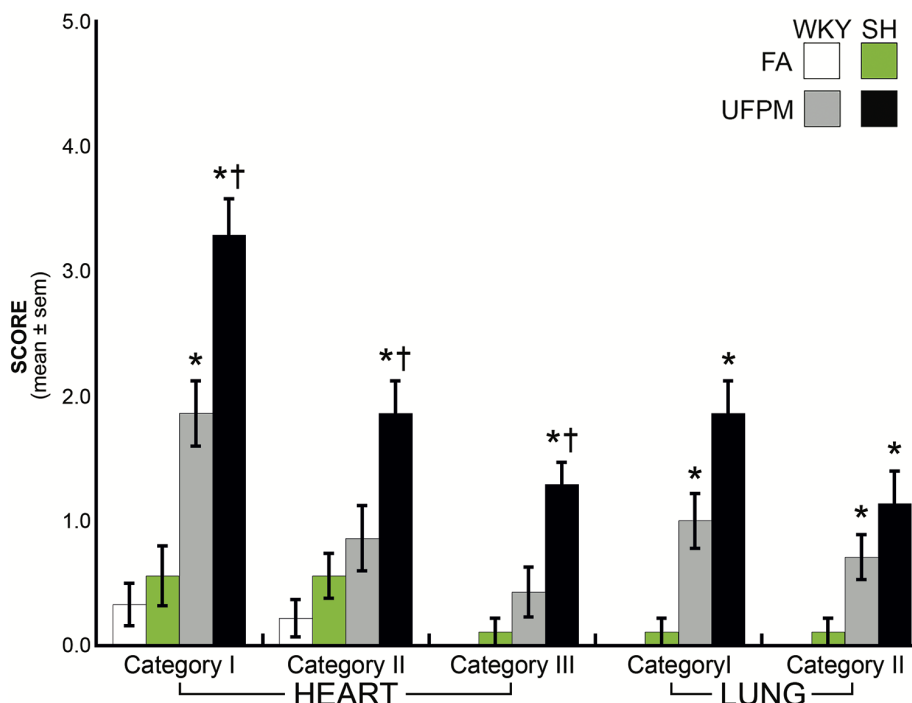


**Figure 3.** UFPM increased microthrombi formation in myocardium and lung. UFPM increased microthrombi in the heart and lung compared to FA. Interestingly, UFPM-exposed SH rats had increased in the heart compared to UFPM-exposed WKY rats. Scores (scale: 0 to 5) were given based on number of aggregates observed per category in one of three samples assessed for each animal. Values are shown as the means  $\pm$  SEM by strain.  $p$ -Values  $\leq 0.05$  were considered significant. \*Significant difference compared to FA within strain-related exposure group. †Significant difference between strains within exposure-related groups.

## OBJECTIVE 2. Characterize UFPM+O<sub>3</sub> impact on microthrombi formation.

There were no strain-related effects on microthrombi formation in heart or lung tissue of FA-exposed rats.

### UFPM-Induced Microthrombi Formation

**Lung.** Overall, UFPM exposure increased category I-II microthrombi in the lung ( $p < 0.001$ ) compared to FA exposure (Fig. 2; Table 2). Within WKY-related exposure groups, UFPM significantly increased category I-II microthrombi ( $p \leq 0.016$ ) compared to FA. Within SH-related exposure groups, UFPM significantly increased category I-II microthrombi ( $p \leq 0.008$ ) compared to FA. UFPM-exposed SH rats displayed increased category I microthrombi ( $p = 0.053$ ) compared to similarly-exposed WKY rats. **Heart.** Overall, UFPM exposure increased category I-III microthrombi in the heart ( $p \leq 0.002$ ) compared to FA exposure (Fig. 2; Table 3). Within WKY-related

exposure groups, UFPM significantly increased category I microthrombi ( $p \leq 0.001$ ) compared to FA. Within SH-related exposure groups, UFPM significantly increased category I-III microthrombi ( $p \leq 0.003$ ) compared to FA. UFPM-exposed SH rats displayed increased category I-III microthrombi ( $p \leq 0.038$ ) compared to similarly-exposed WKY rats.

**TABLE 3**  
Histopathological Measures of the Myocardium

Parameter	WKY				SH			
	FA	UFPM	O <sub>3</sub>	UFPM+O <sub>3</sub>	FA	UFPM	O <sub>3</sub>	UFPM+O <sub>3</sub>
<sup>§</sup> Fibrosis	0.2 $\pm$ 0.2	0.4 $\pm$ 0.2	0.1 $\pm$ 0.1	0.3 $\pm$ 0.1	1.9 $\pm$ 0.3	1.7 $\pm$ 0.3	1.8 $\pm$ 0.2	2.0 $\pm$ 0.2
Nur77	0.0	0.0	0.0	0.0	0.0	0.0	0.0	0.3 $\pm$ 0.1
JunB	0.0	0.0	0.0	0.0	0.0	0.0	0.0	0.4 $\pm$ 0.2
Fibrin-Stabilized Microthrombi								
Category I	0.3 $\pm$ 0.2	1.9 $\pm$ 0.3*	0.4 $\pm$ 0.2	2.6 $\pm$ 0.3*	0.6 $\pm$ 0.2	3.3 $\pm$ 0.3* <sup>§</sup>	1.1 $\pm$ 0.3	4.5 $\pm$ 0.3* <sup>†§</sup>
II	0.2 $\pm$ 0.2	0.9 $\pm$ 0.3	0.4 $\pm$ 0.2	1.8 $\pm$ 0.2*	0.6 $\pm$ 0.2	1.9 $\pm$ 0.3* <sup>§</sup>	1.0 $\pm$ 0.3	2.4 $\pm$ 0.2* <sup>†§</sup>
III	0.0	0.4 $\pm$ 0.2	0.4 $\pm$ 0.2	0.5 $\pm$ 0.2	0.1 $\pm$ 0.1	1.3 $\pm$ 0.2* <sup>§</sup>	0.6 $\pm$ 0.2	1.7 $\pm$ 0.2* <sup>†§</sup>

Note: Sections of the heart were evaluated histologically for interstitial fibrosis, microthrombi; or immunohistochemically for Nur77, nonapoptotic death marker, or JunB, myocardial ischemia marker. Myocardial fibrosis scores (scale: 0 to 5) were assigned based on extent and severity of lesions observed. The number of Nur77 and/or JunB-positive cell clusters within the left ventricle and interventricular septum of a heart section were counted and recorded per section. Microthrombi scores (scale: 0 to 5) were given based on number of aggregates observed per category per lung section for each animal. Values are shown as the means  $\pm$  SEM within strain-related exposure groups.  $p$ -Values  $\leq 0.05$  were considered significant. \*Significant difference from FA within strain-related exposure groups. †Significant difference from O<sub>3</sub> within strain-related exposure groups.

*Heart.* Overall, UFPM exposure increased category I-III microthrombi in the heart ( $p \leq 0.002$ ) compared to FA exposure (Fig. 3; Table 3). Within WKY-related exposure groups, UFPM significantly increased category I microthrombi ( $p \leq 0.001$ ) compared to FA. Within SH-related exposure groups, UFPM significantly increased category I-III microthrombi ( $p \leq 0.003$ ) compared to FA. UFPM-exposed SH rats displayed increased category I-III microthrombi ( $p \leq 0.038$ ) compared to similarly-exposed WKY rats.

#### O<sub>3</sub>-Induced Microthrombi Formation

There were no strain or exposure related-differences in response to O<sub>3</sub> in the lung or heart (Fig. 4 and 5; Table 2 and 3).

#### UFPM+O<sub>3</sub>-Induced Microthrombi Formation

*Lung.* Overall, UFPM+O<sub>3</sub> increased category I-III microthrombi in the lung ( $p \leq 0.004$ ) compared to FA; and category I-III ( $p \leq 0.005$ ) compared to O<sub>3</sub> (Fig. 4; Table 2). Within WKY-related exposure groups, UFPM+O<sub>3</sub> significantly increased category I-II microthrombi ( $p \leq 0.029$ ) compared to FA; and category I-II ( $p \leq 0.040$ ) compared to O<sub>3</sub>. Within SH-related exposure groups, UFPM+O<sub>3</sub> significantly increased category I-III microthrombi ( $p \leq 0.004$ ) compared to FA; and category I-III ( $p \leq 0.034$ ) compared to O<sub>3</sub>. UFPM+O<sub>3</sub>-exposed SH rats displayed increased category I-III microthrombi ( $p \leq 0.028$ ) compared to similarly-exposed WKY rats.

*Heart.* Overall, UFPM+O<sub>3</sub> increased category I-III microthrombi in the heart ( $p < 0.001$ ) compared to FA; and category I-II ( $p < 0.001$ ) compared to O<sub>3</sub> (Fig. 5; Table 3). Within WKY-related exposure groups, UFPM+O<sub>3</sub> significantly increased category I-II microthrombi ( $p \leq 0.001$ ) compared to FA; and category I-II ( $p \leq 0.007$ ) compared to O<sub>3</sub>. Within SH-related exposure groups, UFPM+O<sub>3</sub> significantly increased category I-III microthrombi ( $p < 0.001$ ) compared to FA; and category I-III ( $p \leq 0.028$ ) compared to O<sub>3</sub>. UFPM+O<sub>3</sub>-exposed SH rats displayed increased category I-III microthrombi ( $p \leq 0.038$ ) compared to similarly-exposed WKY rats.

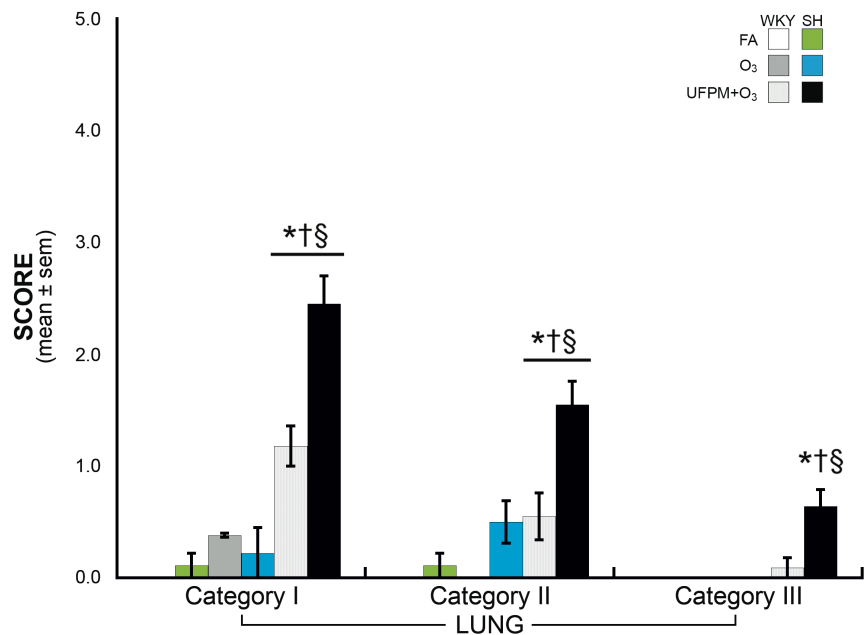


**Figure 4.** UFPM+O<sub>3</sub> increased microthrombi formation in lung. UFPM+O<sub>3</sub>

SH rats had increased microthrombi compared to UFPM+O<sub>3</sub>-exposed WKY rats. Scores (scale: 0 to 5) were given based on number of aggregates observed per category in one of three samples assessed for each animal. Values are shown as the means  $\pm$  SEM by strain.  $p$ -Values  $\leq 0.05$  were considered significant. \*Significant difference compared to FA within strain-related exposure groups. †Significant difference compared to O<sub>3</sub> within strain-related exposure groups. §Significant difference between UFPM+O<sub>3</sub>-exposed WKY and SH rats.

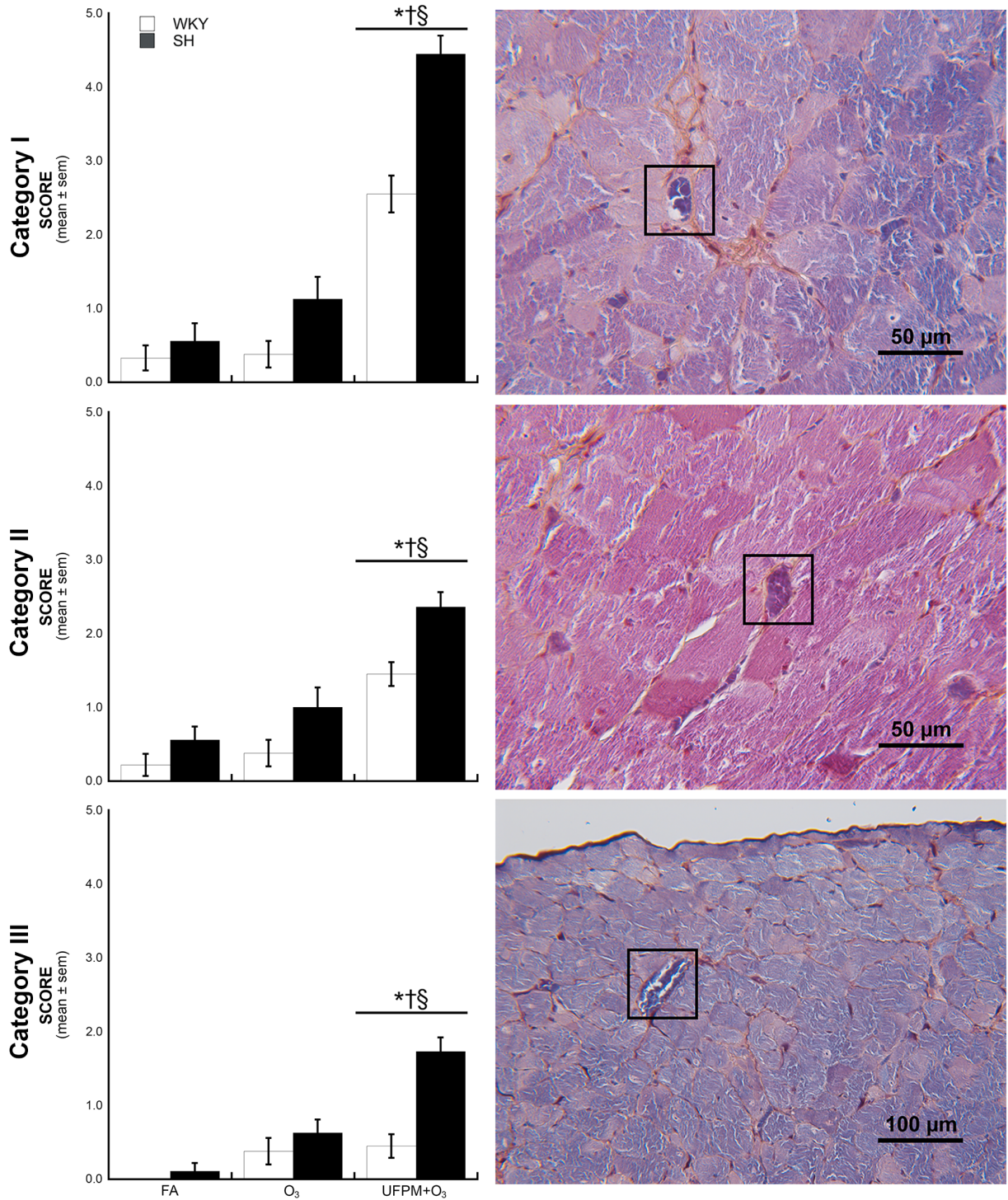


**Figure 5.** UFPM+O<sub>3</sub> increased microthrombi formation in myocardium. Right panel: Representative images of category I-III fibrin-stabilized aggregates observed in left ventricular region of a UFPM+O<sub>3</sub>-exposed SH rat. Left panel: Overall, UFPM+O<sub>3</sub> increased category I-III microthrombi ( $p = 0.000$ ) compared to FA and category I-II ( $p = 0.000$ ) compared to O<sub>3</sub>. Importantly, UFPM+O<sub>3</sub>-SH rats had increased category I-III microthrombi ( $p \leq 0.007$ ) compared to similarly-exposed WKY rats. Scores (scale: 0 to 5) were given based on number of aggregates observed per category in one of three samples assessed for each animal. Values are shown as the means  $\pm$  SEM by strain.  $p$ -Values  $\leq 0.05$  were considered significant. \*Significant difference compared to FA within strain-related exposure groups. †Significant difference compared to O<sub>3</sub> within strain-related exposure groups. §Significant difference between UFPM+O<sub>3</sub>-exposed WKY and

**Objective 3. Define UFPM+O<sub>3</sub> impact on myocardial injury.** Overall, SH rats displayed significantly greater extent of replacement fibrosis ( $p < 0.001$ ) compared to age-matched WKY rats, while there were no exposure effects in either strain (Fig. 6; Table 3). Unfortunately, there were no significant strain- or exposure-related differences for either Nur77 or JunB (Table 3). However, these results do not exclude ischemic injury. Previous epidemiologic studies have demonstrated that increased hospitalizations for cardiovascular-related events, specifically ischemia and infarction, occur one to two days following an increase in daily-levels of ambient PM (6). This suggests that our 8-hour post-exposure time-point was not a sufficient duration for assessment. Importantly, previous studies have shown that ischemic-induced increases in JunB expression is detectable by immunohistochemistry 30-min post-permanent occlusion of the left anterior descending coronary artery in rats (29). While this procedure is an established model of acute myocardial injury, it is not an appropriate model of exposure-related myocardial injuries where time is a critical factor in lesion development.

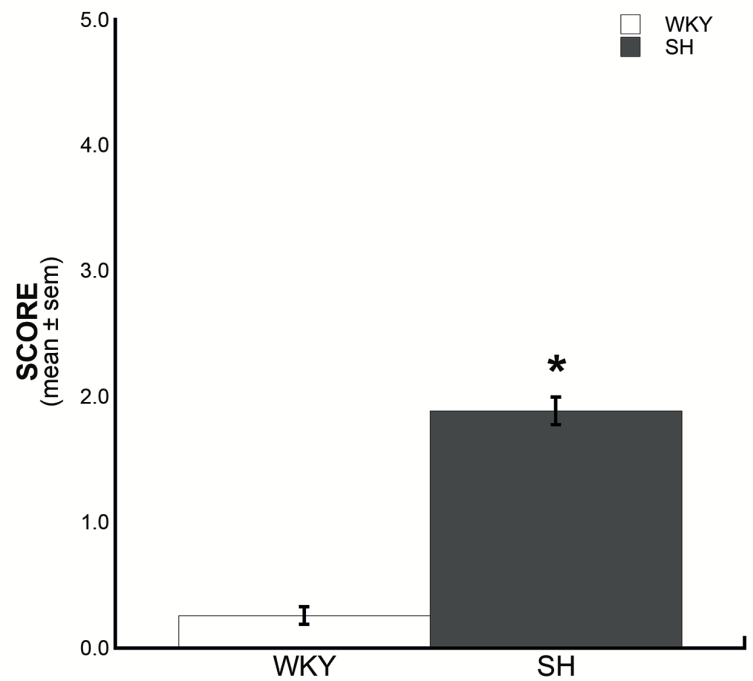


**Figure 6.** Myocardial fibrosis in WKY rat versus SH rats. SH rats display increased fibrosis compared to WKY rats. Scores (scale: 0 to 5) were assigned based on extent and severity of lesions

## 6. DISCUSSION

PM<sub>2.5</sub> and O<sub>3</sub> are ubiquitous air pollutants most often correlated with adverse cardiovascular impacts (30). Epidemiologic data has repeatedly demonstrated that older individuals with pre-existing CVD are at greater risk for air pollution-related cardiopulmonary morbidities and mortalities (1, 2). Growing evidence supports the notion that systemic inflammation, and endothelial injury and dysfunction play a critical role the adverse cardiovascular events associated with short and long term exposure to gaseous and particulate air pollutants (30-32). Especially important for the current study is the strong link between oxidative stress, the generation of ROS and the induction of thrombosis (33). The objective of our present study was to further characterize the mature adult SH rat model of CVD and define the impact of simultaneous exposure to UFPM and O<sub>3</sub> on microthrombi formation within the heart and lungs.

In the current study, we confirmed that mature adult SH rats display CVD-associated cardiac structural remodeling independent of exposure (Table 3; Fig 6). This remodeling was characterized by increasing extent of interstitial expansion and replacement fibrosis within the left ventricle and interventricular septum. This observation is consistent with previous findings of cardiac remodeling and fibrosis in aging humans (34, 35) and SH rats (36-38). The observation of CVD-associated cardiac fibrosis in combination with our previous observations that SH rats display exposure independent ventricular focal organized necrosis, and greater leukocyte/platelet aggregation with stimulation (3) support that the SH rats used this study were undergoing a disease process that was characterized by a history of cardiac injury and remodeling that was associated with an elevated prothrombotic state. This ongoing disease process in combination with a greater airway sensitivity to oxidant stress (3, 25) and the age-dependent onset of super ventricular and ventricular arrhythmias (3, 39), makes the mature adult SH rat more susceptible to air pollution induced myocardial injury.

Both UFPM and UFPM+O<sub>3</sub> exposures increased fibrin-stabilized microthrombi within arterioles, and medium or large arteries within the heart and lungs, with mature adult SH rats being more susceptible to UFPM and UFPM+O<sub>3</sub> compared to age-matched WKY rats. The observation of fibrin-stabilized microthrombi within the arterioles of the lung with UFPM is consistent the generation of ROS or other mediators and the induction of endothelial dysfunction and enhanced thrombosis (33). This pulmonary vascular response is exacerbated with UFPM+O<sub>3</sub> exposure and is greater in severity and extent in the SH rats. The exacerbated pulmonary vascular response in the SH rats is consistent with the elevated baseline thrombosis and increased pulmonary sensitivity to oxidant stress observed in the SH rats (3, 25). The parallel pattern of fibrin-stabilized microthrombi in the heart in WKY and SH rats suggest a link between the exposure related prothrombotic events present in the pulmonary vasculature and the coronary circulation. This link remains undefined and could involve the delivery of blood borne ROS, inflammatory mediators and/or activated platelets to the coronary vessels or the translocation of UFPM particulates into pulmonary circulation and the subsequent deposition in the coronary vessels. Anyone of these processes would likely induce endothelial dysfunction of coronary circulation and contribute to a thrombotic state. The presence of extensive microthrombi that completely occlude small coronary arterioles in SH rats exposed to UFPM+O<sub>3</sub> would produce areas of focal ischemia within the myocardium that could result in the previously described myocardial injury (3).

A critical consideration that we made in designing the current study was the age of the rats to be studied. Aging is a progressive process of decline that leads to compromised physiological function, even in the absence of disease (40, 41). Age-related deterioration is particularly notable in the cardiopulmonary system. In the lung, aging alters immune responses, antioxidant defenses, and airway receptor activity (42). Structural changes can also occur, impairing lung compliance, and increasing work associated with breathing (43). In the heart, aging promotes adverse changes in cardiac structure and function, which is presumably related to a decline in cardioprotective molecular mechanisms [for full review see Obas et al. (44)]. Importantly, age-related changes in the heart lower the threshold for CVD development. Therefore, anticipated increases in older populations will coincide with an increasing burden of CVD. In fact, epidemiologic data indicates that by 2030, nearly half of the U.S. adult population will have some form of CVD (5). The mature adult rats used in this study demonstrated multiple age related changes including myocardial remodeling and fibrosis, and cardiac arrhythmias making them appropriate surrogates for modeling air pollution-induced cardiovascular responses in the aging human.

Two factors are critical to evaluation of our previous (3, 25) and current data, these are; (1) the relative delivered

dose of UFPM to the airway, and (2) the PAH composition of the UFPM and UFPM+O<sub>3</sub> atmospheres.

We employed a high concentration of particles in our UFPM atmospheres, much higher than typical ambient levels of PM<sub>0.1</sub>. For toxicologic assessments, however, it is more critical to evaluate dose-equivalent responses rather than replicate atmospheric pollutant concentrations (45). Because particle deposition is dependent on anatomic and physiologic characteristics, dose levels in a rodent are substantially lower than a human when exposed to similar pollutant concentrations (46). Thus, significantly higher concentrations are necessary to achieve human-equivalent dose levels in a rodent model of exposure. To demonstrate the relevance of the UFPM concentration used in the current study, we performed a dosimetric comparison between UFPM, a high ambient concentration of traffic-related PM<sub>0.1</sub>, and the current NAAQS for PM<sub>2.5</sub> (25). Particle dosimetry predictions indicated that the experimental concentration of UFPM was relevant to that of a high ambient concentration of traffic-related PM<sub>0.1</sub> and an acute 24-hour exposure to PM<sub>2.5</sub> at the NAAQS for a human at rest and with light activity (25).

The experimental UFPM was produced by a premixed flame particle generating system, and contained vapor- and particulate-phase PAHs. The premixed flame particle generating system is ideal for toxicity testing of combustion-generated PM<sub>0.1</sub> because it is reproducible, allows for compositional modification, and eliminates the composition and size-fraction variability associated with field samples. Previously, Chan et al. reported that biphenyls and naphthalene derivatives dominated both the vapor and particulate phases of the UFPM atmosphere (49). Although biphenyls were abundant in vapor-phase UFPM+O<sub>3</sub>, only two chemically stable poly-substituted naphthalene derivatives were identified. In contrast, the particulate-phase UFPM+O<sub>3</sub> chemical composition was completely distinct from UFPM alone, and devoid of any PAHs with demonstrated carcinogenic capacity (25). Previous studies indicated that atmospheric reactions of O<sub>3</sub> with surface-adsorbed PAHs occur in a somewhat indiscriminate manner and promotes PAH degradation (13, 50, 51). For example, quinoline, a biologically relevant PAH-derivative commonly formed in vehicular combustion engines (52), was identified in vapor- and particulate-phases of UFPM, but was not present in either phase of UFPM+O<sub>3</sub>. Due to its oxidative capacity, O<sub>3</sub> quickly reacts with and degrades PAHs. This oxidative reaction is accelerated when PAHs are deposited on a solid surface (53). In diesel exhaust PM, PAH half-lives range from 15 to 120 minutes (51). The rate of PAH conversion by O<sub>3</sub> is dependent on the electrophilic reactivity of the compound. For example, quinones are highly reactive to electrophilic reactions, and thus, particularly susceptible to ozonolysis (54). Importantly, PAH ozonolysis yields a complex mixture of oxidized products including hydroxyl radicals, aldehydes, carboxylic acids, and hydrogen peroxides (54). The production of these compounds would directly increase the particle's oxidant capacity, and conceivably, its biologic potency. In the current study we showed (3, 25) that the presence of O<sub>3</sub> dramatically altered the PAH composition of UFPM in the UFPM+O<sub>3</sub> experimental atmosphere (Table 1). Therefore, the biological effects resulting from UFPM+O<sub>3</sub> exposure in part results from O<sub>3</sub> and PAH interactions and the change in PAH composition.

We previously reported that the combination of UFPM and O<sub>3</sub> increased the extent of lung injury in WKY rats beyond an "additive" effect of the single- pollutant exposures combined, suggesting that biologic potency was enhanced (3, 25). These observations are similar to previously reported acute lung responses following exposure to combined pollutants (15, 47, 48). In contrast, while there was a trend for the UFPM+O<sub>3</sub> exposure to have elevated levels of thrombi in the lung and heart compared to UFPM exposure alone, these increases were at most additive. This difference may be due to the fact that O<sub>3</sub> would be present at the airway surface where it can directly contribute to injury, but would not be present within the vasculature where thrombi formation would occur.

### **Integration of Results**

Our current results, in combination with the results of our initial study in the same cohort of rats (3) a complex picture arises of the cascade of events that eventually leads to myocardial injury in SH rats exposed to UFPM+O<sub>3</sub> (Fig. 7).

The Animal Model: Though mature adult WKY and SH rats, both, exhibit similar baseline cardiac arrhythmias, SH rats have baseline characteristics that make them more susceptible to air pollution induced myocardial injury. This increase susceptibility is associated with the current observation that mature adult SH rats display greater interstitial expansion and replacement fibrosis within left ventricle and interventricular septum, and our previous

observations that SH rats display ventricular focal organized necrosis, greater leukocyte/platelet aggregation with stimulation and increased pulmonary sensitivity to oxidant stress.

The Exposure Model: Evidence from some studies suggest that atmospheric interactions between PM and O<sub>3</sub> may enhance the adverse effects resulting from exposure (15, 47, 48). O<sub>3</sub> reacts with PAHs contained in combustion-derived UFPM in the atmosphere to produce a potentially more toxic profile of oxidant-derived reaction products (Table 1; Fig. 7).

The Lung: O<sub>3</sub> reacts with antioxidants and lipid components of the airway lining fluid (ALF) to produce ozonation products that result in injury of airway epithelial cells (AECs) and inflammation. SH rats were more sensitive to these O<sub>3</sub>-induced effects. The inhalation of UFPM by itself resulted in increased fibrin-stabilized microthrombi within pulmonary arterioles of both WKY and SH rats consistent with UFPM deposition on the surface of the AECs of terminal airways and potentially the surface of alveolar epithelial cells (AlvECs) and the subsequent activation of platelets (Fig. 7). The inhalation of UFPM+O<sub>3</sub> resulted in greater fibrin-stabilized microthrombi within pulmonary arterioles and small pulmonary arteries of SH rats indicating a greater thrombotic response.

The Heart: Inhalation of UFPM by itself resulted in increased fibrin-stabilized microthrombi within small ventricular arterioles of both WKY and SH rats. SH rats had more microthrombi in small ventricular arterioles and arteries that were more severe than those present in WKY rats. Inhalation of UFPM+O<sub>3</sub> resulted in greater fibrin-stabilized microthrombi within ventricular arterioles and small ventricular arteries of SH rats indicating a greater thrombotic response that was associated. The greater UFPM+O<sub>3</sub> induced ventricular microthrombi responses in the WKY and SH rats was associated with an increased number and severity of premature ventricular contractions (PVCs) and an increased number of atrioventricular block (AVB) events. In SH rats the greater UFPM+O<sub>3</sub> induced ventricular microthrombi response was associated with the presence of acute necrosis. This observation is consistent with the possibility that the severe microthrombi in SH rats exposed to UFPM+O<sub>3</sub> produced areas of focal ischemia within the myocardium that results in myocardial injury.

Lung-Heart Interactions. The activation of lung sensory nerves following exposure to O<sub>3</sub> in SH rats and UFPM+O<sub>3</sub> in SH and WKY rats sends signals to the brainstem where the signals are integrated and result in pulmonary and cardiovascular reflexes (Fig. 7). The pulmonary reflexes result primarily in breathing pattern changes, including rapid shallow breathing (RSB) and augmented breaths (ABs). The cardiovascular reflexes result in changes in the parasympathetic (PNS) and sympathetic (SNS) nervous system outflow to the heart. The PNS and SNS innervate the sino-atrial node (SA node), atrioventricular node (AV node) and the myocardium. The inhalation of O<sub>3</sub> and UFPM+O<sub>3</sub> by SH rats and UFPM+O<sub>3</sub> by WKY rats, decreases heart rate (HR), increases heart rate variability (HRV), increases the high frequency (HF) of HRV, and increases the number AVB events, all of which are consistent with increased PNS outflow to the SA and AV node (Fig. 7). However, other HRV parameters, including increases in the ratio of LF to HF (LF/HF) and decreases in approximate entropy (ApEn) along with increases the number of PVCs are consistent with the co-activation of the SNS (Fig. 7). The co-activation of the SNS is especially pronounced in SH rats exposed to UFPM+O<sub>3</sub>, where the initial PNS-induced decrease in HR and increase in HRV are blunted as exposure progresses. It is likely that the activation of sensory nerves within the ventricular myocardium are activated by the focal ischemia that is produced by the microthrombi and PVCs. Activation of these sensory nerves have been shown to increase SNS and decrease PNS outflow to the heart (55-58).

Another potentially critical lung-heart interaction is the extent that microthrombi produced in the lung and UFPM deposited in the lung are translocated to the systemic and coronary circulation (Fig. 7). The translocation of UFPM to the heart could potentially induce endothelial dysfunction, platelet activation, and microthrombi formation, thereby, further contributing to the vascular occlusion of coronary vessels (Fig. 7).

**Relevance.** This work improves scientific understanding of the adverse effects of simultaneous combined-pollutant exposure and provides novel insight into the association between ambient air pollution and increased cardiac morbidity and mortality in mature adult individuals with CVD. This will aid CARB in developing and evaluating air pollution standards in the context of the exacerbated adverse cardiovascular events that are induced by the combined exposure to O<sub>3</sub> and UFPM in individuals with preexisting cardiovascular disease and highlights the need to develop an ambient air pollution metric that better predicts the adverse health effects

induced by combined pollutant exposure. This might require targeted controlled human and animal exposure studies, as well as new epidemiology studies that focus on pollutant interactions and their effects on cardiovascular and other outcomes.

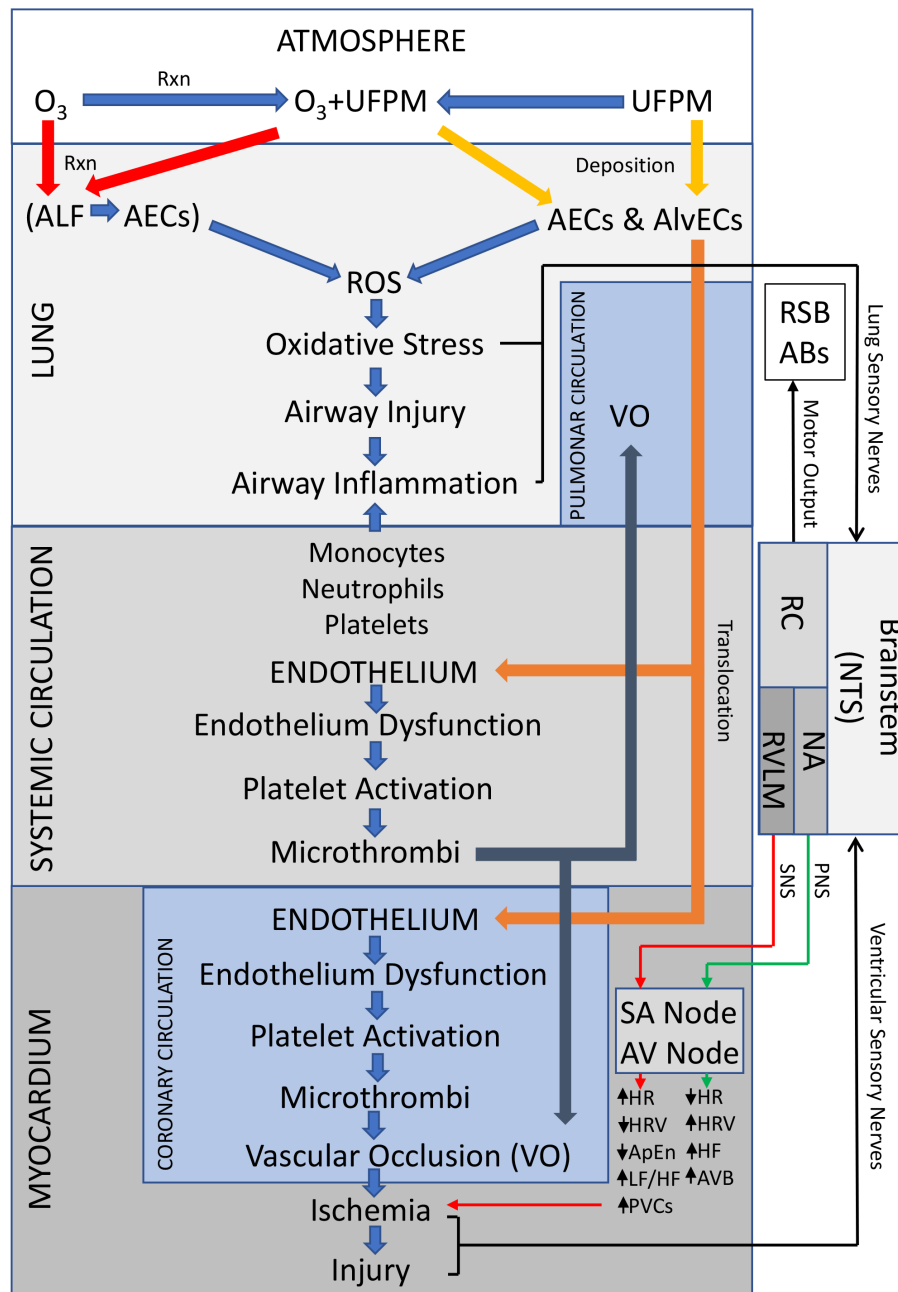


**Figure 7.** Integration of results of the current study (CARB# 17RD011, Combined Exposures to Ultrafine Particulate Matter and Ozone: Characterization of Particulate Deposition, Pulmonary Oxidant Stress and Myocardial Injury; PI Schelegle) and those from our previous study (CARB# 13-311, Co-exposure to UFPM and O<sub>3</sub>: Pulmonary C fiber and platelet activation in decreased HRV; PI: Tablin) illustrating the integration of multiple mechanisms that contribute to adverse cardiovascular effects in rats, but may also be present in older humans with cardiovascular disease.. Abbreviations: ABs, augmented breaths; AECs, airway epithelial cells; ALF, airway lining fluid; AlVECs, alveolar epithelial cells; ApEn, approximate entropy; AVB, atrioventricular block; AV Node, atrioventricular node; HR, heart rate; HRV, heart rate variability; HF, high frequency; LF/HF, ratio of low to high frequency; NA, nucleus ambiguus; NTS, nucleus tractus solitarius; PNS, parasympathetic nervous system; PVCs, premature ventricular contractions; RSB, rapid shallow breathing; RC, respiratory center; ROS, reactive oxygen species; RVLM, rostral ventrolateral

## 7. RECOMMENDATIONS

**Time.** Results from the present study clearly demonstrate that exposure-related effects that have different time courses must be examined at different time-points. In the present study, all endpoints were examined eight-hours post-exposure. However, our results clearly demonstrate that certain endpoints need to be examined at different time-points, outlined below.

Particle deposition: Examine immediately (+0-hour) following exposure period. We recommend using a 1-hour exposure period to limit clearance.

Nrf2 antioxidant expression: Examine at one (+24-hour) and two (+48-hour) days post-exposure. PM-induced increases have been detected 24-hours post-exposure, but maximum expression occurred 48-hours post-exposure (59, 60).

Myocardial ischemia: Examine at one (+24-hour) and two (+48-hour) days post-exposure. Previous epidemiologic studies have demonstrated that increased hospitalizations for cardiovascular-related events, including ischemia and infarction, occur one to two days following an increase in daily-levels of ambient PM (6).

**Examine role of endothelial dysfunction.** Previously, we demonstrated that simultaneous exposure to UFPM+O<sub>3</sub> resulted in similar airway injury and inflammation, changes in platelet activation and platelet-leukocyte interactions, and increased cardiac arrhythmias in mature adult rats with and without CVD. However, we do not detect significant differences between mature adult rats with CVD and those without CVD in fibrin-stabilized microthrombi in the pulmonary and coronary circulation and acute cellular necrosis. These findings are consistent with epidemiologic evidence that older individuals with CVD are increasingly susceptible to exposure-related adverse health effects. To better understand the link between thrombosis and myocardial injury, we recommend that future investigations examining the dose-response relationship of simultaneous combined-pollutant exposures incorporate measures of endothelial activation and dysfunction, as well as microthrombi formation.

**Examine the toxicity of O<sub>3</sub> altered UFPM in isolation.** Results of the current study suggest that the change in the UFPM PAH composition following the reaction with O<sub>3</sub> increases the toxicity. Therefore, we recommend that future investigations examine the response of UFPM and UFPM reacted with O<sub>3</sub>, but without the O<sub>3</sub> present. As above these studies should include measures of endothelial activation and dysfunction and microthrombi formation in mature adult rats with and without CVD.

## 8. GLOSSARY OF TERMS, ABBREVIATIONS, AND SYMBOLS

ABs	augmented breaths
AECs	airway epithelial cells
ALF	airway lining fluid
AlvECs	alveolar epithelial cells
ApEn	approximate entropy
AVB	atrioventricular block
AV Node	atrioventricular node
CV	cardiovascular
CVD	cardiovascular disease
CF	cardiac fibrosis
ECG	electrocardiogram
EC/OC	elemental carbon to organic carbon ratio
FA	filtered air
HMOX-1	hemoxygenase-1
HR	heart rate
HRV	heart rate variability
HF	high frequency
LF/HF	ratio of low to high frequency
NA	nucleus ambiguus
NTS	nucleus tractus solitarius
O <sub>3</sub>	ozone
PNS	parasympathetic nervous system
PM	particulate matter
PM0.1	particulate matter 0.1 μm or less in diameter
PM2.5	particulate matter 2.5 μm or less in diameter
PTAH	phosphotungstic acid-hematoxylin
PAHs	poly-aromatic hydrocarbons
PVCs	premature ventricular contractions
RSB	rapid shallow breathing
ROS	reactive oxygen species
Rxn	reaction
RC	respiratory center
RT	room temperature
RVLM	rostral ventrolateral medulla
SH	Spontaneous Hypertensive rats
SOD	superoxide dismutase
SNS	sympathetic nervous system
PM0.1	ultrafine particulate matter, aerodynamic diameter < 0.1 μm
UFPM	ultrafine particulate matter (surrogate particle)
VO	vascular occlusion
UFPM+O <sub>3</sub>	co-pollutant atmosphere, simultaneous exposure
WKY	Wistar-Kyoto rats

## 9. REFERENCES

1. Samet JM, Dominici F, Curriero FC, Coursac I, Zeger SL. Fine particulate air pollution and mortality in 20 u.S. Cities, 1987-1994. *N Engl J Med* 2000;343(24):1742-1749.
2. Peters A, Dockery DW, Muller JE, Mittleman MA. Increased particulate air pollution and the triggering of myocardial infarction. *Circulation* 2001;103(23):2810-2815.
3. Tablin F. Co-exposure to UFPM and O<sub>3</sub>: Pulmonary c fiber and platelet activation in decreased hrv. California Air Resources Board: Contract #13-311, 2017.
4. Ljungman PL, Mittleman MA. Ambient air pollution and stroke. *Stroke* 2014;45(12):3734-3741.
5. Benjamin EJ, Blaha MJ, Chiuve SE, Cushman M, Das SR, Deo R, de Ferranti SD, Floyd J, Fornage M, Gillespie C, et al. Heart disease and stroke statistics-2017 update: A report from the american heart association. *Circulation* 2017;135(10):e146-e603.
6. Brook RD, Rajagopalan S, Pope CA, Brook JR, Bhatnagar A, Diez-Roux AV, Holguin F, Hong Y, Luepker RV, Mittleman MA, et al. Particulate matter air pollution and cardiovascular disease: An update to the scientific statement from the american heart association. *Circulation* 2010;121(21):2331-2378.
7. Rich DQ, Balmes JR, Frampton MW, Zareba W, Stark P, Arjomandi M, Hazucha MJ, Costantini MG, Ganz P, Hollenbeck-Pringle D, et al. Cardiovascular function and ozone exposure: The multicenter ozone study in older subjects (moses). *Environ Int* 2018;119:193-202.
8. Bell ML, McDermott A, Zeger SL, Samet JM, Dominici F. Ozone and short-term mortality in 95 us urban communities, 1987-2000. *JAMA* 2004;292(19):2372-2378.
9. Hoek G, Boogaard H, Knol A, de Hartog J, Slottje P, Ayres JG, Borm P, Brunekreef B, Donaldson K, Forastiere F, et al. Concentration response functions for ultrafine particles and all-cause mortality and hospital admissions: Results of a european expert panel elicitation. *Environ Sci Technol* 2010;44(1):476-482.
10. Lanzinger S, Schneider A, Breitner S, Stafoggia M, Erzen I, Dostal M, Pastorkova A, Bastian S, Cyrus J, Zscheppang A, et al. Ultrafine and fine particles and hospital admissions in central europe. Results from the ufereg study. *Am J Respir Crit Care Med* 2016;194(10):1233-1241.
11. Hoek G, Schwartz JD, Groot B, Eilers P. Effects of ambient particulate matter and ozone on daily mortality in rotterdam, the netherlands. *Arch Environ Health* 1997;52(6):455-463.
12. Pönkä A, Savela M, Virtanen M. Mortality and air pollution in helsinki. *Arch Environ Health* 1998;53(4):281-286.
13. Pitts JN, Lokensgard DM, Ripley PS, VAN Cauwenberghe KA, VAN Vaeck L, Shaffer SD, Thill AJ, Belser WL. "Atmospheric" Epoxidation of benzo[a]pyrene by ozone: Formation of the metabolite benzo[a]pyrene-4,5-oxide. *Science* 1980;210(4476):1347-1349.
14. Kozumbo WJ, Agarwal S. Induction of dna damage in cultured human lung cells by tobacco smoke arylamines exposed to ambient levels of ozone. *Am J Respir Cell Mol Biol* 1990;3(6):611-618.
15. Madden MC, Richards JH, Dailey LA, Hatch GE, Ghio AJ. Effect of ozone on diesel exhaust particle toxicity in rat lung. *Toxicol Appl Pharmacol* 2000;168(2):140-148.
16. Rouse RL, Murphy G, Boudreaux MJ, Paulsen DB, Penn AL. Soot nanoparticles promote biotransformation, oxidative stress, and inflammation in murine lungs. *Am J Respir Cell Mol Biol* 2008;39(2):198-207.
17. Li N, Sioutas C, Cho A, Schmitz D, Misra C, Sempf J, Wang M, Oberley T, Froines J, Nel A. Ultrafine particulate pollutants induce oxidative stress and mitochondrial damage. *Environ Health Perspect* 2003;111(4):455-460.
18. Dye JA, Lehmann JR, McGee JK, Winsett DW, Ledbetter AD, Everitt JI, Ghio AJ, Costa DL. Acute pulmonary toxicity of particulate matter filter extracts in rats: Coherence with epidemiologic studies in utah valley residents. *Environ Health Perspect* 2001;109 Suppl 3:395-403.
19. Li N, Alam J, Venkatesan MI, Eiguren-Fernandez A, Schmitz D, Di Stefano E, Slaughter N, Killeen E, Wang X, Huang A, et al. Nrf2 is a key transcription factor that regulates antioxidant defense in macrophages and epithelial cells: Protecting against the proinflammatory and oxidizing effects of diesel exhaust chemicals. *J Immunol* 2004;173(5):3467-3481.
20. Lucking AJ, Lundback M, Mills NL, Faratian D, Barath SL, Pourazar J, Cassee FR, Donaldson K, Boon NA, Badimon JJ, et al. Diesel exhaust inhalation increases thrombus formation in man. *Eur Heart J* 2008;29(24):3043-3051.
21. Tablin F, den Hartigh LJ, Aung HH, Lame MW, Kleeman MJ, Ham W, Norris JW, Pombo M, Wilson DW. Seasonal influences on caps exposures: Differential responses in platelet activation, serum cytokines and xenobiotic gene expression. *Inhal Toxicol* 2012;24(8):506-517.

22. Wilson DW, Aung HH, Lame MW, Plummer L, Pinkerton KE, Ham W, Kleeman M, Norris JW, Tablin F. Exposure of mice to concentrated ambient particulate matter results in platelet and systemic cytokine activation. *Inhal Toxicol* 2010;22(4):267-276.
23. Kilkenny C, Browne WJ, Cuthill IC, Emerson M, Altman DG. Improving bioscience research reporting: The arrive guidelines for reporting animal research. *PLoS Biol* 2010;8(6):e1000412.
24. 89-544. PL. The animal welfare act - public law 89-544. In: Agriculture. USDo, editor. United States Code: U.S. Federal Government;1966.
25. Wong EM, Walby WF, Wilson DW, Tablin F, Schelegle ES. Ultrafine particulate matter combined with ozone exacerbates lung injury in mature adult rats with cardiovascular disease. *Toxicol Sci* 2018;163(1):140-151.
26. Herner JD, Aw J, Gao O, Chang DP, Kleeman MJ. Size and composition distribution of airborne particulate matter in northern california: I--particulate mass, carbon, and water-soluble ions. *J Air Waste Manag Assoc* 2005;55(1):30-51.
27. Shackelford C, Long G, Wolf J, Okerberg C, Herbert R. Qualitative and quantitative analysis of nonneoplastic lesions in toxicology studies. *Toxicol Pathol* 2002;30(1):93-96.
28. Sutherland KM, Edwards PC, Combs TJ, Van Winkle LS. Sex differences in the development of airway epithelial tolerance to naphthalene. *Am J Physiol Lung Cell Mol Physiol* 2012;302(1):L68-81.
29. Sabatasso S, Mangin P, Fracasso T, Moretti M, Docquier M, Djonov V. Early markers for myocardial ischemia and sudden cardiac death. *Int J Legal Med* 2016;130(5):1265-1280.
30. Bourdrel T, Bind MA, Béjot Y, Morel O, Argacha JF. Cardiovascular effects of air pollution. *Arch Cardiovasc Dis* 2017;110(11):634-642.
31. Münzel T, Gori T, Al-Kindi S, Deanfield J, Lelieveld J, Daiber A, Rajagopalan S. Effects of gaseous and solid constituents of air pollution on endothelial function. *Eur Heart J* 2018;39(38):3543-3550.
32. Pope CA, Bhatnagar A, McCracken JP, Abplanalp W, Conklin DJ, O'Toole T. Exposure to fine particulate air pollution is associated with endothelial injury and systemic inflammation. *Circ Res* 2016;119(11):1204-1214.
33. Gu SX, Stevens JW, Lentz SR. Regulation of thrombosis and vascular function by protein methionine oxidation. *Blood* 2015;125(25):3851-3859.
34. Kane AE, Howlett SE. Differences in cardiovascular aging in men and women. *Adv Exp Med Biol* 2018;1065:389-411.
35. Keller KM, Howlett SE. Sex differences in the biology and pathology of the aging heart. *Can J Cardiol* 2016;32(9):1065-1073.
36. Linz D, Hohl M, Mahfoud F, Reil JC, Linz W, Hübschle T, Juretschke HP, Neumann-Häflin C, Rütten H, Böhm M. Cardiac remodeling and myocardial dysfunction in obese spontaneously hypertensive rats. *J Transl Med* 2012;10:187.
37. Levick SP, McLarty JL, Murray DB, Freeman RM, Carver WE, Brower GL. Cardiac mast cells mediate left ventricular fibrosis in the hypertensive rat heart. *Hypertension* 2009;53(6):1041-1047.
38. Conrad CH, Brooks WW, Hayes JA, Sen S, Robinson KG, Bing OH. Myocardial fibrosis and stiffness with hypertrophy and heart failure in the spontaneously hypertensive rat. *Circulation* 1995;91(1):161-170.
39. Scridon A, Gallet C, Arisha MM, Oréa V, Chapuis B, Li N, Tabib A, Christé G, Barrès C, Julien C, et al. Unprovoked atrial tachyarrhythmias in aging spontaneously hypertensive rats: The role of the autonomic nervous system. *Am J Physiol Heart Circ Physiol* 2012;303(3):H386-392.
40. Janssens JP, Pache JC, Nicod LP. Physiological changes in respiratory function associated with ageing. *Eur Respir J* 1999;13(1):197-205.
41. Zeleznik J. Normative aging of the respiratory system. *Clin Geriatr Med* 2003;19(1):1-18.
42. Wang L, Green FH, Smiley-Jewell SM, Pinkerton KE. Susceptibility of the aging lung to environmental injury. *Semin Respir Crit Care Med* 2010;31(5):539-553.
43. Green F, Pinkerton K. Environmental determinants of lung aging. In: Harding R, Pinkerton K, Plopper C, editors. The lung: Development, aging and the environment. London: Academic Press;2004. p. 377-395.
44. Obas V, Vasan RS. The aging heart. *Clin Sci (Lond)* 2018;132(13):1367-1382.
45. Oberdörster G, Oberdörster E, Oberdörster J. Nanotoxicology: An emerging discipline evolving from studies of ultrafine particles. *Environ Health Perspect* 2005;113(7):823-839.
46. Brown JS, Wilson WE, Grant LD. Dosimetric comparisons of particle deposition and retention in rats and humans. *Inhal Toxicol* 2005;17(7-8):355-385.

47. Bouthillier L, Vincent R, Goegan P, Adamson IY, Bjarnason S, Stewart M, Guénette J, Potvin M, Kumarathasan P. Acute effects of inhaled urban particles and ozone: Lung morphology, macrophage activity, and plasma endothelin-1. *Am J Pathol* 1998;153(6):1873-1884.
48. Elder AC, Gelein R, Finkelstein JN, Cox C, Oberdörster G. Pulmonary inflammatory response to inhaled ultrafine particles is modified by age, ozone exposure, and bacterial toxin. *Inhal Toxicol* 2000;12 Suppl 4:227-246.
49. Chan JK, Fanucchi MV, Anderson DS, Abid AD, Wallis CD, Dickinson DA, Kumfer BM, Kennedy IM, Wexler AS, Van Winkle LS. Susceptibility to inhaled flame-generated ultrafine soot in neonatal and adult rat lungs. *Toxicol Sci* 2011;124(2):472-486.
50. Van Cauwenberghe K, Van Vaeck L. Toxicological implications of the organic fraction of aerosols: A chemist's view. *Mutat Res* 1983;116(1):1-20.
51. Van Vaeck L, Van Cauwenberghe K. Conversion of polycyclic aromatic hydrocarbons on diesel particulate matter upon exposure to ppm levels of ozone. *Atmos Environ* 1984;18:323-328.
52. Jakober C, Riddle S, Robert M, Destailats H, Charles M, Green P, Kleeman M. Quinone emissions from gasoline and diesel motor vehicles. *Environ Sci Technol* 2007;41:4558-4554.
53. Pitts J, Paur H, Zielinska B, Arey J, Winer A, Ramdahl T, Mejia V. Factors influencing the reactivity of polycyclic aromatic hydrocarbons adsorbed on filters and ambient pom with ozone. *Chemosphere* 1986;15:675-685.
54. Bernatek E. Ozonolysis of naphthoquinones. *Tetrahedron* 1958;4:213-222.
55. Ludbrook J. Cardiovascular reflexes from cardiac sensory receptors. *Aust N Z J Med* 1990;20(4):597-606.
56. Fu L, Longhurst J. Regulation of cardiac afferent excitability in ischemia. *Handbook of Experimental Pharmacology* 2009;194:185-225.
57. Foreman RD, Blair RW, Holmes HR, Armour JA. Correlation of ventricular mechanosensory neurite activity with myocardial sensory field deformation. *Am J Physiol* 1999;276(4):R979-989.
58. Veelken R, Glabasnia A, Stetter A, Hilgers KF, Mann JF, Schmieder RE. Epicardial bradykinin b2 receptors elicit a sympathoexcitatory reflex in rats. *Hypertension* 1996;28(4):615-621.
59. Chan JK, Kodani SD, Charrier JG, Morin D, Edwards PC, Anderson DS, Anastasio C, Van Winkle LS. Age-specific effects on rat lung glutathione and antioxidant enzymes after inhaling ultrafine soot. *Am J Respir Cell Mol Biol* 2013;48(1):114-124.
60. Chan JK, Charrier JG, Kodani SD, Vogel CF, Kado SY, Anderson DS, Anastasio C, Van Winkle LS. Combustion-derived flame generated ultrafine soot generates reactive oxygen species and activates nrf2 antioxidants differently in neonatal and adult rat lungs. *Part Fibre Toxicol* 2013;10:34.